Journal of Non-Crystalline Solids 409 (2015) 49–53

Contents lists available at ScienceDirect

Journal of Non-Crystalline Solids

journal homepage: www.elsevier.com/ locate/ jnoncrysol

Ab initio study of Si doping effects in Pd–Ni–P bulk metallic glass

J.A. Reyes-Retana *, G.G. Naumis

Departamento de Física-Química, Instituto de Física, Universidad Nacional Autónoma de México (UNAM), Apartado Postal 20-364, 01000 México, Distrito Federal, Mexico

ARTICLE INFO

Article history:
Received 25 August 2014
Received in revised form 1 November 2014
Accepted 7 November 2014
Available online xxxx

Keywords:
Bulk metallic glasses;
Ab-initio calculations;
Topological properties

ABSTRACT

In order to understand the improved glass formation ability of bulk metallic glass due to Si doping, several structures were obtained by means of density functional theory. The results indicate that Si enters mainly as a substitute for P in the clusters, inducing a shoving effect in the P–P random network. The corresponding electronic properties indicate an enhanced cluster stabilization due to an electronic mechanism, which reduces the density of states at the Fermi level.

1. Introduction

Bulk metallic glasses (BMGs) exhibit unique electrical, chemical, mechanical and magnetic properties [1]. They have very useful mechanical properties, which are unique in contrast with the corresponding crystalline structures. At the moment, there is a wide range of multicomponent BMG alloys [2]. However, one of the most difficult problems in order to achieve industrial production is the high cooling speeds required to generate metallic glasses. In glasses, this tendency is measured by the so-called glass formation ability [3]. For covalent glasses, the Phillips rigidity theory provides a beautiful framework to understand glass forming abilities and chemical composition [4]. For glasses with no directional bondings, the application of such theory is still a very active field of research [5–9]. In spite of this, there are some empirical criteria about how the glass formation ability depends upon several parameters [10–12]. As a result, it was once believed that monocomponent metallic glasses were impossible to form. Such feat was only very recently achieved by using a simple but very fast cooling technique [13].

An important milestone in the understanding on how to control glass formation abilities was the experimental observation of group IV doping effects on metallic glasses [14,15]. In particular, here we are interested on the famous $Pd_{40}Ni_{40}P_{20}$ bulk metallic glasses, which was first prepared by Drehman et al. in 1982 [16,17]. Later on, Chen et al. included a minor percent of Si (2–4%) which significantly improved the glass-formation ability and mechanical properties [14,15]. Although this is a significant step in the search of new and improved glasses, there is still a lack of theoretical understanding in the mechanism behind such remarkable effect. A comprehension of this effect can open the way to design metallic glasses with improved glass formation abilities.

To open such question, in a previous work we have made a study of how Si influences crystals with compositions near the $Pd_{40}Ni_{40}P_{20}$ glass [18]. However, there are still no available numerical studies on the doped glasses. Here we provide such study by using density functional theory (DFT).

Our work is mainly guided by following earlier attempts to describe the structure of $Pd_{40}Ni_{40}P_{20}$ BMG [19] in terms of building blocks (BBs) within the glass. Most of the BBs in the $Pd_{40}Ni_{40}P_{20}$ are made from slightly deformed tricapped trigonal prisms [2], although it is not clear how they are connected [20]. Some clues have been obtained using density functional theory [19,20].

In this article, we present a description of the resulting structure and electronic properties of Si doped $Pd_{40}Ni_{40}P_{20}$ metallic glasses. The layout of the work is the following. We start describing the methodology used to generate the glasses. Then a study of the structural effects is made, and the calculations of the electronic properties are presented. Finally the conclusion is given.

2. Materials and methods

These *ab initio* calculations were done by using the Quantum ESPRESSO [21] plane wave DFT and density functional perturbation theory (DFPT) code, available under the GNU Public License [22]. Scalar relativistic and non-spin polarized calculation were performed. A plane-wave basis set with the cutoff of 612 eV was used. Also, an ultrasoft pseudo-potential [23] from the standard distribution generated using a modified RRKJ [24] approach, and the generalized gradient approximation [25] (GGA) for the exchange-correlation functional in its PBE parametrization [26] was used. All atomic positions and lattice parameters of the supercells were optimized using the conjugate gradient method.

* Corresponding author.
E-mail address: angelreyes@fisica.unam.mx (J.A. Reyes-Retana).

http://dx.doi.org/10.1016/j.jnoncrysol.2014.11.011
0022-3093/

Table 1
Densities of the models obtained with cells of 200 atoms in the $Pd_{40}Ni_{40}P_{20-x}Si_x$ systems.

$Pd_{40}Ni_{40}P_{20-x}Si_x$	Density (g/cm^3)
x = 0	8.93 (9.21[a]) (9.4[b])
x = 0.5	8.99
x = 1.0	8.92
x = 1.5	8.96
x = 2.0	9.02

[a] Numerical simulation value reported by Kumar et al. [19].
[b] Experimental value [31].

The convergence for energy was chosen as 10^{-7} eV between two consecutive steps and the maximum forces acting are smaller than 0.05 eV/Å. The stress in the periodic direction is lower than 0.01 GPa in all cases. Once the structures were relaxed, the electronic density of states were calculated with the tetrahedral method [27].

To build the models, two methods were used. One starts with building a $Pd_{40}Ni_{40}P_{20}$ glass model from the BBs taken from the related crystals as follows. A starting orthorhombic supercell of $Pd_{40}Ni_{40}P_{20}$ with 120 atoms was made, where all P atoms are centered in the tricapped prism BBs and with no P–P connections. The starting connections BBs are mainly face-sharing chains with some vertex- and edge-sharing connections. Once the $Pd_{40}Ni_{40}P_{20}$ model was built, some P atoms were replaced by Si with the required concentration. The supercell was heated at 3000 K in 200 time steps then it was cooled to 0 K in 150 time steps with the cooling rate of 2×10^{16} K/s. The Γ-point was used to perform integration over k vectors. The Verlet algorithm with a time step of 1 fs to integrate the Newton's equations of motion was used. The temperature was controlled by using the velocity rescaling method. Finally, all coordinates and cell parameters were relaxed with the convergence parameters for the energy and forces described above.

The second model follows the method proposed by Kumar et. al. [19] for building the pure $Pd_{40}Ni_{40}P_{20}$ glass. One starts from a random configuration of Pd, Ni and P atoms with a given concentration inside a cubic cell. The calculations were made with three different numbers of atoms: 60, 110 and 200 atoms, although here we only present the results for 200 atoms. The supercell was heated at 3000 K in 400 time steps, then it was cooled to 0 K in 300 time steps with the cooling rate of 1×10^{16} K/s. The Γ-point was used to perform integration over k vectors. The Verlet algorithm with a time step of 1 fs to integrate the Newton's equations of motion was used. The temperature was also controlled by using the velocity rescaling method. Finally, all coordinates and cell parameters were relaxed. The substitution of P by Si was done with 1, 2, 3, and 4 atoms on each starting cubic cell. Then the completed computational process described above was applied for all samples. The resulting densities for the biggest supercells are reported in Table 1.

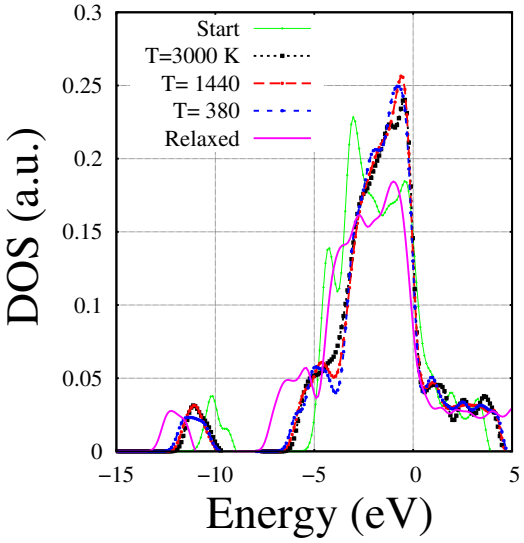

Fig. 2. Evolution of the density of states of $Pd_{40}Ni_{40}P_{20}$ during the thermal procedure.

The typical numerical radial distribution functions $g(r)$ obtained by such process are shown in Fig. 1. It is important here to remark that in most of other *ab initio* works [19,28,29], the simulation time is about tens of picoseconds, while in this work it was near to 1 ps. To test the effects of such high cooling speed, in Figs. 2 and 3 we present the evolution of the density of states (DOS) for $Pd_{40}Ni_{40}P_{20}$. In the DOS evolution for the thermal history, it is clearly seen that the original structure changes a lot with the first heating, while due to the high cooling speed, the DOS is slightly modified as cooling is performed. However, when the structure is relaxed, it is possible to observe that the DOS is strongly modified. In particular, the evolution towards lower energies is clear, specially for the lowest band, which corresponds to P s states and p hybridized states with Ni and Pd, as we will discuss later on. Notice how the transition metal bands, which are close to the Fermi energy (set at $E = 0$), are less modified. This suggests that in the melt, there is already an incipient formation of transition metal clusters, as is known to occur in such kind of systems [30]. This can explain the resilient behavior of the system with respect to the cooling rate. On the other hand, we performed simulations at slower cooling rates as seen in Fig. 3. The most important result here is the good reproducibility for different cooling rates. In fact, the obtained DOS is very similar to the

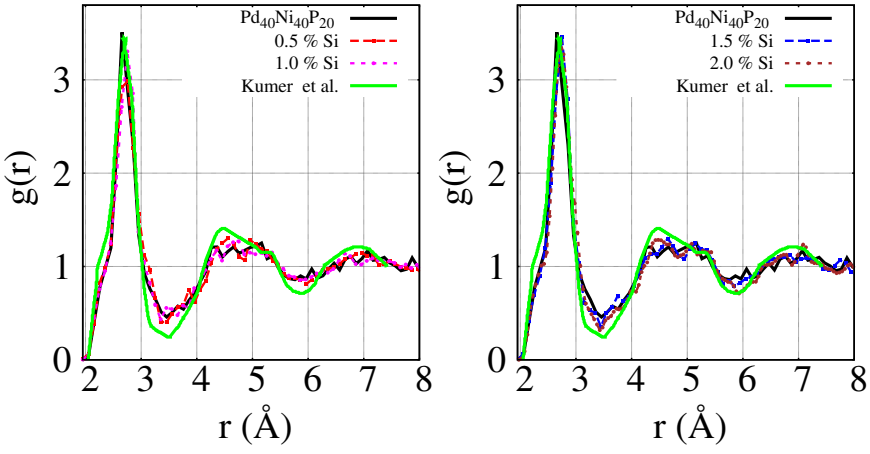

Fig. 1. Total radial distribution function of $Pd_{40}Ni_{40}P_{20}$, and the effects of a 0.5, 1, 1.5 and 2% Si inclusion, for a system of 200 atoms. Also, the experimental (green) RDF is shown, obtained from [19]. (For interpretation of the references to color in this figure legend, the reader is referred to the web version of this article.)

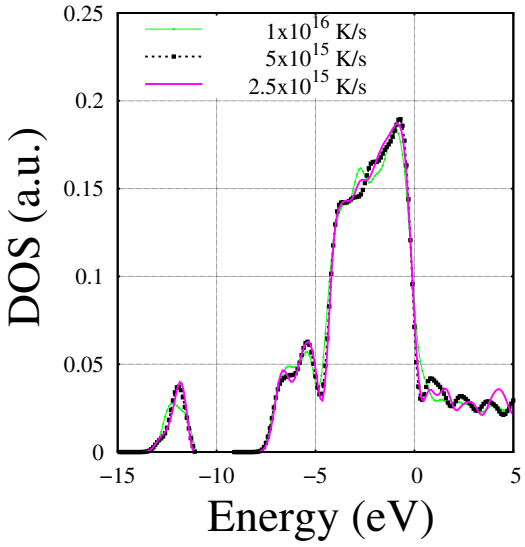

Fig. 3. Comparison of the density of states for $Pd_{40}Ni_{40}P_{20}$ using different cooling rates.

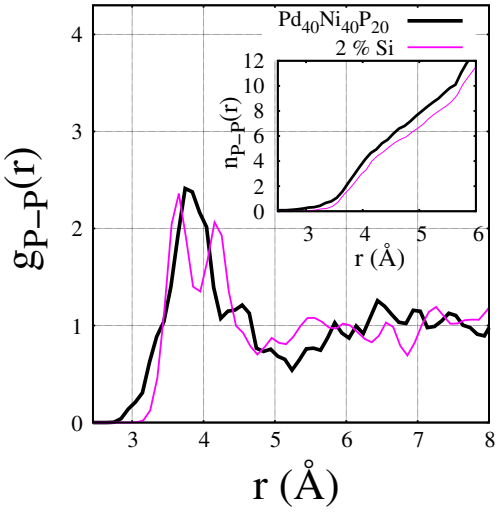

Fig. 4. P–P partial radial distribution function of $Pd_{40}Ni_{40}P_{20}$ and the effect of a 2% Si inclusion. The inset is the integral over the area of the P–P partial distribution. This plot was obtained by averaging over three samples.

ones of glassy clusters [20] and related crystalline compounds [18,20]. Furthermore, the two-body correlations, coordination numbers, densities and local clusters obtained by this method are in reasonable agreement with other experimental and numerical simulations [19], making us confident in the methodology.

3. Structural properties

To validate the proposed methodology, we used pure $Pd_{40}Ni_{40}P_{20}$ glass as a benchmark tool. In particular, we compared our results with the experimental and numerical radial distribution functions $g(r)$ detailed in Ref. [19], as well as with the coordination numbers of each kind of atoms and local cluster structure reported in Ref. [19]. Our numerical results of the second method are in closer agreement with the experimental data (see for example Fig. 1) than those obtained with the first method based in joining crystalline BBs. Although the general features of $g(r)$ are well reproduced with the BBs, in general there are more peaks indicating a tendency for crystallization. Thus, it seems that the method based on an initial randomization is better suited to describe the resulting structures. Therefore, we decided to apply this method to deal with Si doping.

In Fig. 1 we present the effects on $g(r)$ of small Si doping, compared with the experimental and numerical results for the pure $Pd_{40}Ni_{40}P_{20}$ glass. Due to the low quantity of Si, there are no significant changes.

The main effects of Si are seen when the partial radial distribution function P–P contribution ($g_{P-P}(r)$) is plotted as a function of Si doping, as seen in Fig. 4. In the pure $Pd_{40}Ni_{40}P_{20}$ glass, the highest peak of $g_{P-P}(r)$ occurs at $r = 3.75$ Å. After a small 2% Si addition, the peak splits dramatically into two peaks at $r = 3.65$ Å and at $r = 4.15$ Å. The inset in Fig. 4 shows the integral over the area of the P–P partial distribution. To gain further insight, one can make an analysis of the generated structures based on the geometrical distances obtained from the pair-correlations of P–P and P–Si. Such analysis can be made by plotting all P and Si sites, as seen in Fig. 5. Then, we draw a fictitious line/stick to join all P and Si which have a distance lower than 4 Å, since according to Fig. 4, the maximum of the P–P correlation is contained in such interval. An analysis of the random fictitious network generated by using this procedure is seen in Fig. 5, and indicates a shoving effect around the Si. In fact, the distance from a Si to the first P atom was found to be around $r \approx 4.10$ Å, which is bigger than the distance of the main peak in the P–P correlation. This is in agreement with a previous report made by our group in related crystalline compounds [18].

Concerning the clusters, we have found that Si basically enters at the center of the clusters as a replacement of P. However, the shoving effect of Si has a great impact in the coordination number of P. In Fig. 6, we

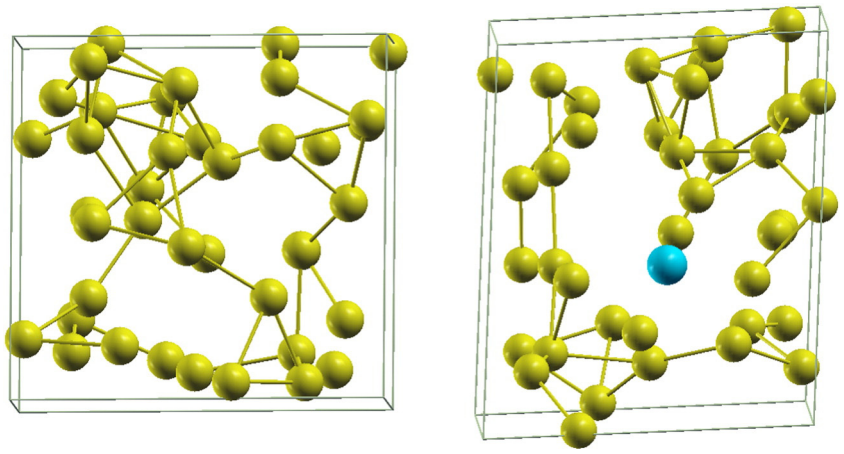

Fig. 5. Random network generated by the P (in yellow) and Si (in blue) positions for the glass models. The connections are fictitious and displayed only for illustration purposes. Such connections are shown for those P–P or P–Si distances lower that 4 Å. Notice how the Si atom is isolated, while P atoms are pushed away around it. (For interpretation of the references to color in this figure legend, the reader is referred to the web version of this article.)

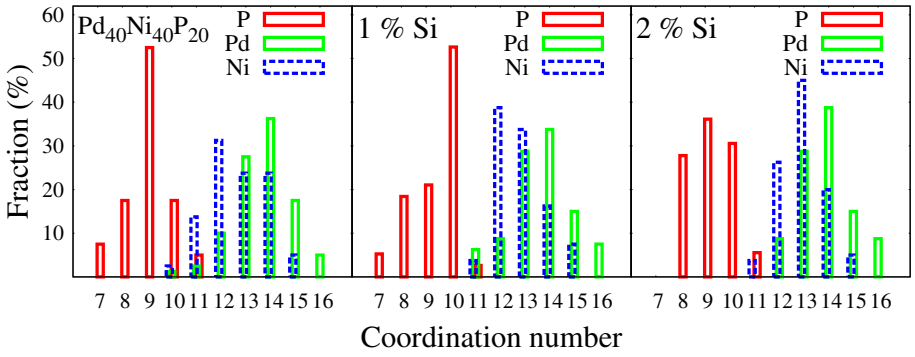

Fig. 6. Effect of a 1% and 2% Si inclusion in the coordination number for the Pd–Ni–P bulk metallic.

present the effect of a small Si inclusion. For the pure $Pd_{40}Ni_{40}P_{20}$ glass, our model roughly gives the same results found by Kumar et. al. [19]. In such case, nearly 60% of P atoms have a coordination of 9, with a small percentage of 7 and 8. Around 20% have a coordination of 10. When a 2% of Si is added, the 9 coordinated P atoms fall to 30%, while 10 coordinated increase to nearly 35%. Furthermore, 7 coordinated P are not seen anymore and 8 coordinated P increases from 20% to 30%. Thus, the connectivity is dramatically changed with a small Si doping.

4. Electronic properties

Once the glass models were obtained, we calculated the DOS as described in the Materials and method section. In Fig. 7 we present the corresponding results as a function of doping, as well as a zoom around the Fermi energy. For the pure $Pd_{40}Ni_{40}P_{20}$ glass, our results are similar to those obtained in the related crystals [18]. Basically, the peaks between $E = -15$ eV and $E = -10$ eV are produced by P s states. A second bump is seen between $E = -7.5$ eV and $E = -5$ eV, which are due to a mix of P p states and Pd and Ni p states. The biggest bump between $E = -5$ eV and the Fermi energy corresponds basically to d states of transition metals. The Si doping has three effects. The first is the raising of a new peak close to $E = -10$ eV. This new peak is due to the Si s states, which have a higher energy than P s states. The second is a sharpening of the first P s states peak, due to the changes in the P centered clusters. The third and most important effect is a decreasing of the DOS at the Fermi level, which seems to indicate an electronic

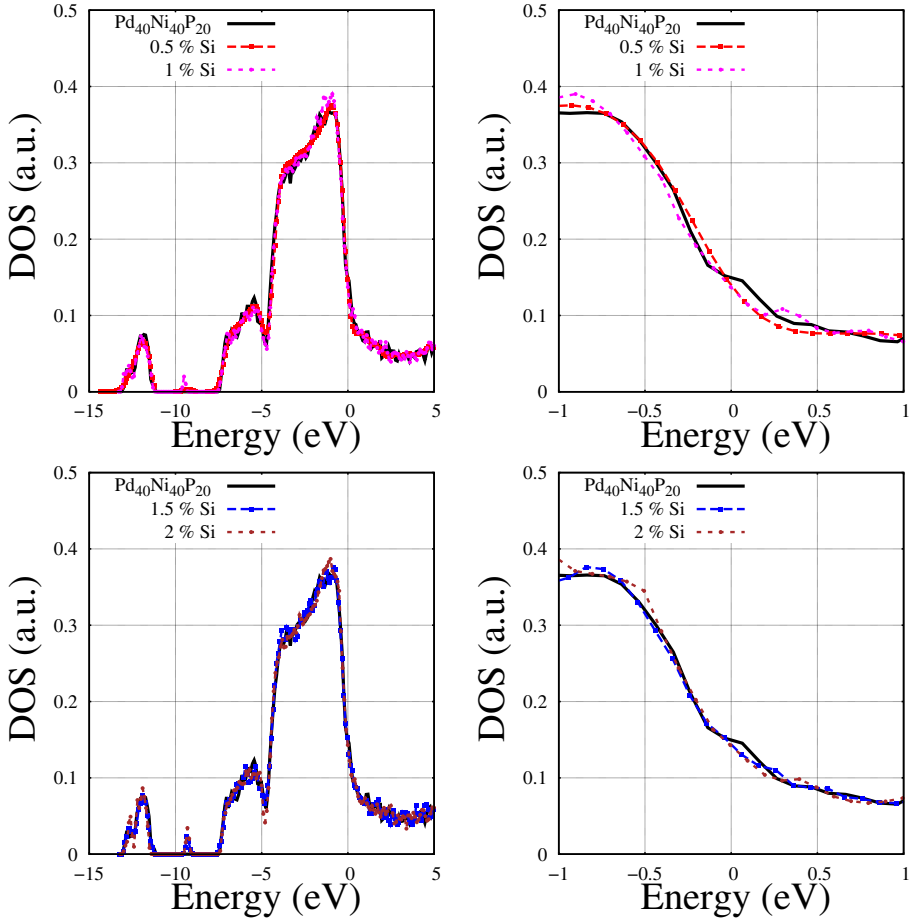

Fig. 7. Effect of the Si inclusion in the electronic density of states of Pd–Ni–P bulk metallic glass. The plot at the right corresponds to a zoom around the Fermi energy, which here corresponds to $E = 0$.

stabilization of the structure, as was suggested in the related crystalline compounds [18].

5. Conclusions

In conclusion, we have investigated the effects of Si doping in the $Pd_{40}Ni_{40}P_{20}$ glass by using density functional theory. We found that Si produces a shoving effect in the random network of P centered clusters. This shoving is due to the size mismatch of Si atoms. This shoving induces dramatic changes in the P coordination, by increasing the connectivity of P with surrounding clusters, as was previously concluded in related crystalline compounds [18]. All these effects produce a decreasing electronic density of states at the Fermi level, suggesting an electronic stabilization mechanism behind the improved glass formation ability of covalent doped metallic glasses.

These changes in coordinations due to the shoving effect, can be responsible for the improved glass formation ability, as has been put forward by Phillips rigidity theory [32–35,11,12,36–38].

Acknowledgment

The authors thank J.C. Phillips for enlightening discussions and suggesting us the study of this interesting system. JARR acknowledges support from DGAPA-UNAM. We have benefited from the use of computational resources at the DGTIC-UNAM (Mixtli) and Centro Nacional de Supercómputo (Thubat-Kaal) at San Luis Potosí. This work was supported by DGPA-PAPIIT IN-102513 project.

References

[1] M.F. Ashby, A.L. Greer, Metallic glasses as structural materials, Scr. Mater. 54 (3) (2006) 321–326.
[2] Akihisa Inoue, Stabilization of metallic supercooled liquid and bulk amorphous alloys, Acta Mater. 48 (1) (2000) 279–306.
[3] C. Suryanarayana, Akihisa Inoue, Bulk Metallic Glasses, CRC Press, 2011.
[4] J.C. Phillips, Topology of covalent non-crystalline solids I: short-range order in chalcogenide alloys, J. Non-Cryst. Solids 34 (2) (1979) 153–181.
[5] Adrian Huerta, Gerardo G. Naumis, Darsh T. Wasan, Douglas Henderson, Andrij Trokhymchuk, Attraction-driven disorder in a hard-core colloidal monolayer, J. Chem. Phys. 120 (3) (2004).
[6] A. Huerta, G.G. Naumis, Rigidity aspects of the glass transition, J. Non-Cryst. Solids 329 (1–3) (2003) 100–103 (7th Int. Workshop on Non-Crystalline Solids).
[7] Adrián Huerta, Gerardo G. Naumis, Role of rigidity in the fluid–solid transition, Phys. Rev. Lett. 90 (Apr 2003) 145701.
[8] Adrián Huerta, Gerardo G. Naumis, Evidence of a glass transition induced by rigidity self-organization in a network-forming fluid, Phys. Rev. B 66 (Nov 2002) 184204.
[9] A. Huerta, G.G. Naumis, Relationship between glass transition and rigidity in a binary associative fluid, Phys. Lett. A 299 (2002) 660–665.
[10] John C. Mauro, Morten M. Smedskjaer, Statistical mechanics of glass, J. Non-Cryst. Solids 396–397 (0) (2014) 41–53.
[11] John C. Mauro, Statistics of modifier distributions in mixed network glasses, J. Chem. Phys. 138 (12) (2013).
[12] John C. Mauro, Morten M. Smedskjaer, Unified physics of stretched exponential relaxation and Weibull fracture statistics, Physica A 391 (23) (2012) 6121–6127.
[13] Li Zhong, Jiangwei Wang, Hongwei Sheng, Ze Zhang, Scott X. Mao, Formation of monatomic metallic glasses through ultrafast liquid quenching, Nature 512 (7513) (2014) 177–180.
[14] N. Chen, D.V. Louzguine-Luzgin, G.Q. Xie, T. Wada, A. Inoue, Influence of minor si addition on the glass-forming ability and mechanical properties of Pd40Ni40P20 alloy, Acta Mater. 57 (9) (2009) 2775–2780.
[15] Y.Q. Zeng, A. Inoue, N. Nishiyama, M.W. Chen, Ni-rich Ni–Pd–P bulk metallic glasses with significantly improved glass-forming ability and mechanical properties by si addition, Intermetallics 18 (9) (2010) 1790–1793.
[16] A.J. Drehman, A.L. Greer, D. Turnbull, Bulk formation of a metallic glass: Pd40Ni40P20, Appl. Phys. Lett. 41 (8) (1982).
[17] H.W. Kui, Al L. Greer, D. Turnbull, Formation of bulk metallic glass by fluxing, Appl. Phys. Lett. 45 (1984) 615.
[18] J.A. Reyes-Retana, G.G. Naumis, The effects of si substitution on the glass forming ability of Ni–Pd–P system, a DFT study on crystalline related clusters, J. Non-Cryst. Solids 387 (2014) 117–123.
[19] Vijay Kumar, T. Fujita, K. Konno, M. Matsuura, M.W. Chen, A. Inoue, Y. Kawazoe, Atomic and electronic structure of $Pd_{40}Ni_{40}P_{20}$ bulk metallic glass from ab initio simulations, Phys. Rev. B 84 (Oct 2011) 134204.
[20] Tsunehiro Takeuchi, Daisuke Fukamaki, Hidetoshi Miyazaki, Kazuo Soda, Masashi Hasegawa, Hirokazu Sato, Uichiro Mizutani, Takahiro Ito, Shinichi Kimura, Electronic structure and stability of the Pd–Ni–P bulk metallic glass, Mater. Trans. 48 (6) (2007) 1292–1298.
[21] Paolo Giannozzi, Stefano Baroni, Nicola Bonini, Matteo Calandra, Roberto Car, Carlo Cavazzoni, Davide Ceresoli, Guido L. Chiarotti, Matteo Cococcioni, Ismaila Dabo, Andrea Dal Corso, Stefano de Gironcoli, Stefano Fabris, Guido Fratesi, Ralph Gebauer, Uwe Gerstmann, Christos Gougoussis, Anton Kokalj, Michele Lazzeri, Layla Martin-Samos, Nicola Marzari, Francesco Mauri, Riccardo Mazzarello, Stefano Paolini, Alfredo Pasquarello, Lorenzo Paulatto, Carlo Sbraccia, Sandro Scandolo, Gabriele Sclauzero, Ari P. Seitsonen, Alexander Smogunov, Paolo Umari, Renata M. Wentzcovitch, Quantum espresso: a modular and open-source software project for quantum simulations of materials, J. Phys. Condens. Matter 21 (39) (2009) 395502.
[22] GNU General Public License, Free software foundation, GNU Project1991.
[23] David Vanderbilt, Soft self-consistent pseudopotentials in a generalized eigenvalue formalism, Phys. Rev. B 41 (Apr 1990) 7892–7895.
[24] Andrew M. Rappe, Karin M. Rabe, Efthimios Kaxiras, J.D. Joannopoulos, Optimized pseudopotentials, Phys. Rev. B 41 (Jan 1990) 1227–1230.
[25] John P. Perdew, J.A. Chevary, S.H. Vosko, Koblar A. Jackson, Mark R. Pederson, D.J. Singh, Carlos Fiolhais, Atoms, molecules, solids, and surfaces: applications of the generalized gradient approximation for exchange and correlation, Phys. Rev. B 46 (Sep 1992) 6671–6687.
[26] John P. Perdew, Kieron Burke, Matthias Ernzerhof, Generalized gradient approximation made simple, Phys. Rev. Lett. 77 (Oct 1996) 3865–3868.
[27] Peter E. Blöchl, O. Jepsen, O.K. Andersen, Improved tetrahedron method for brillouin-zone integrations, Phys. Rev. B 49 (Jun 1994) 16223–16233.
[28] Murat Durandurdu, Ab initio modeling of metallic Pd80Si20 glass, Comput. Mater. Sci. 65 (2012) 44–47.
[29] H.W. Sheng, W.K. Luo, F.M. Alamgir, J.M. Bai, E. Ma, Atomic packing and short-to-medium-range order in metallic glasses, Nature 439 (7075) (2006) 419–425.
[30] J.L. Aragón, D. Romeu, A. Gómez, Higher-dimensional approach to a unified growth model for crystals, quasicrystals, and multiply twinned particles, Phys. Rev. B 44 (Jul 1991) 584–592.
[31] Osami Haruyama, Thermodynamic approach to free volume kinetics during isothermal relaxation in bulk Pd–Cu–Ni–P20 glasses, Intermetallics 15 (5–6) (2007) 659–662 (Advanced Intermetallic Alloys and Bulk Metallic Glasses 6th International Workshop on Advanced Intermetallic and Metallic Materials).
[32] J.C. Phillips, Stretched exponential relaxation in molecular and electronic glasses, Rep. Prog. Phys. 59 (9) (1996) 1133.
[33] J.C. Phillips, Slow dynamics in glasses: a comparison between theory and experiment, Phys. Rev. B 73 (Mar 2006) 104206.
[34] J.C. Phillips, Microscopic aspects of stretched exponential relaxation (SER) in homogeneous molecular and network glasses and polymers, J. Non-Cryst. Solids 357 (22–23) (2011) 3853–3865.
[35] Roger C. Welch, John R. Smith, Marcel Potuzak, Xiaoju Guo, Bradley F. Bowden, T.J. Kiczenski, Douglas C. Allan, Ellyn A. King, Adam J. Ellison, John C. Mauro, Dynamics of glass relaxation at room temperature, Phys. Rev. Lett. 110 (Jun 2013) 265901.
[36] G.G. Naumis, J.C. Phillips, Bifurcation of stretched exponential relaxation in microscopically homogeneous glasses, J. Non-Cryst. Solids 358 (5) (2012) 893–897.
[37] Hugo M. Flores-Ruiz, Gerardo G. Naumis, J.C. Phillips, Heating through the glass transition: a rigidity approach to the boson peak, Phys. Rev. B 82 (Dec 2010) 214201.
[38] Richard Kerner, Gerardo G. Naumis, Stochastic matrix description of the glass transition, J. Phys. Condens. Matter 12 (8) (2000) 1641.